

Highly Symmetric and Extremely Compact Multiple Winding Microtubes by a Dry Rolling Mechanism

Somayeh Moradi,* Ehsan Saei Ghareh Naz, Guodong Li, Nooshin Bandari, Vineeth Kumar Bandari, Feng Zhu, Horst Wendrock, and Oliver G. Schmidt*

Rolled-up nanotechnology has received significant attention to self-assemble planar nanomembranes into 3D micro and nanotubular architectures. These tubular structures have been well recognized as novel building blocks in a variety of applications ranging from microelectronics and nanophotonics to microbatteries and microrobotics. However, fabrication of multiwinding microtubes with precise control over the winding interfaces, which is crucial for many complex applications, is not easy to achieve by existing materials and technologies. Here, a dry rolling approach is introduced to tackle this challenge and create tight windings in compact and highly symmetric cylindrical microstructures. This technique exploits hydrophobicity of fluorocarbon polymers and the thermal expansion mismatch of polymers and inorganic films upon thermal treatment. Quality parameters for rolled-up microtubes, against which different fabrication technologies can be benchmarked are defined. The technique offers to fabricate long freestanding multiwinding microtubes as well as hierarchical architectures incorporating rolled-up wrinkled nanomembranes. This work presents an important step forward toward the fabrication of more complex but well-controlled microtubes for advanced high-quality device architectures.


Rolled-up tubular devices reported so far very often address applications, which rely on only a small number of windings.^[1d,e,3,5,7] Devices with a larger number of windings such as large-area rolled-up energy storage elements^[8] and microtube inductors^[9] have also been demonstrated, but in this case the tightness and quality of the windings has not been critical to build the devices. Still, fabrication of high-quality multiwinding microtubes is a crucial requirement for applications with more complex functionalities such as rolled-up metamaterial optical fibers,^[10] hyperlenses,^[11] and 3D cylindrical photonic crystals.^[12] Intense research has been conducted in recent years toward these applications, but the inability of the current roll-up mechanisms to provide interfacial defect-free multiple rotation microtubes has prevented engineering of the very same. Providing high-quality winding interfaces will also increase mechanical stability and ensure high yield fabrication of rolled-up

Over the last couple of decades enormous efforts have been made to design, fabricate, and optimize functional micro/nanostructures with desirable size, morphology, and shape. Rolled-up nanotechnology as an elegant approach to self-assemble planar patterned nanomembranes into 3D micro and nanotubular device architectures by built-in differential strain has received increasing attention.^[1] Rolled-up tubular architectures are key to many innovative building blocks in a variety of application scenarios such as compact electronic elements,^[2] optical ring resonators,^[3] lab-in-a-tube,^[4] microtubular biosensors,^[5] and rolled-up magnetic architectures.^[6]

microtubular devices, which in turn will open up a wide variety of engineering and technological applications.

Generally, the stress releasing process for rolling up strained nanomembranes involves wet etching of a sacrificial layer introduced into the structure between the strained nanomembrane and the substrate. This often means employing harsh chemicals^[13] that can cause heavy damage to the active device layers, thus putting severe limitations on materials choice and processing parameters for the rolled-up structures. Roll-up strategies also include exploiting polymeric sacrificial layers^[14]

S. Moradi, E. S. G. Naz, Dr. G. Li, N. Bandari, V. K. Bandari, Dr. F. Zhu, Prof. O. G. Schmidt
Material Systems for Nanoelectronics
Chemnitz University of Technology
Reichenhainer Straße 70, Chemnitz 09107, Germany
E-mail: s.moradi@ifw-dresden.de; o.schmidt@ifw-dresden.de

 The ORCID identification number(s) for the author(s) of this article can be found under <https://doi.org/10.1002/admi.201902048>.

© 2020 The Authors. Published by WILEY-VCH Verlag GmbH & Co. KGaA, Weinheim. This is an open access article under the terms of the Creative Commons Attribution License, which permits use, distribution and reproduction in any medium, provided the original work is properly cited.

DOI: 10.1002/admi.201902048

S. Moradi, E. S. G. Naz, Dr. G. Li, N. Bandari, V. K. Bandari, Dr. F. Zhu, Prof. O. G. Schmidt
Center for Materials
Architectures and Integration of Nanomembranes (MAIN)
Chemnitz University of Technology
Rosenberg Str. 6, Chemnitz 09126, Germany

S. Moradi, E. S. G. Naz, Dr. G. Li, N. Bandari, V. K. Bandari, Dr. F. Zhu, Prof. O. G. Schmidt
Institute for Integrative Nanosciences
Leibniz IFW Dresden
Helmholtzstraße 20, Dresden 01069, Germany

Dr. H. Wendrock
Institute for Complex Materials
Leibniz IFW Dresden
Helmholtzstraße 20, Dresden 01069, Germany

which enable people to use mild organic solvents as etchants, or applying dry etching processes^[15] to avoid damaging effects typically caused by wet chemistry. However, none of these approaches has been able to effectively control and minimize the winding interfacial defects generated during the etching process, especially when a large number of windings is needed in a microtubular device architecture.

Here, we demonstrate an approach based on the adhesion–delamination phenomenon at the interface of dissimilar materials^[16] and the elimination of the need of the sacrificial layer to be etched away during the rolling process. Although delamination at the interface of different classes of materials such as polymers/metals is commonly known to cause catastrophic failure in microelectronics and MEMS devices,^[17] we exploit this “failure mode” to establish a dry platform for curling strained nanomembranes into a new class of rolled-up microtubular structures. The dry self-rolling technique relies on the introduction of an antiadhesive polymeric film between the strained nanomembrane and the holding substrate. Exploiting the hydrophobicity feature of this polymeric film and the thermal expansion difference of the polymer and deposited inorganic films upon heating^[18] leads to an upward delamination of the nanomembranes and a subsequent roll-up process. As the central element of this method we employ amorphous fluorocarbon (FC) polymers (which are nowadays widely used for release-layer technologies^[19]) as low surface energy films for the deposition of strained layer stacks, which are then rolled-up as nanomembrane materials into compact tight-winding microtubes.

Because FC polymers have extremely low surface free energy providing strong nonadhesiveness, the deposition of high-quality thin films needs to be carefully optimized. For instance, the nanomembrane layer materials are deposited at low temperature to minimize thermal expansion mismatch between the polymeric layer and the inorganic films. In this way, the deposited nanomembranes effectively bond to the FC layer surface and the adhesion is high enough to prevent crack formation although the deposited layer stacks are highly strained. The large coefficient thermal expansion (CTE) mismatch between the polymer layers and the strained inorganic nanomembrane layers causes large thermally induced stress to the nanomembranes upon heating up the substrate to elevated temperatures. This extra thermal stress overcomes the weak molecular forces between polymer and nanomembrane and results in the detachment and roll-up of the nanomembrane from the host substrate.

In the following, we present the process for creating highly compact rolled-up microtubes consisting of large numbers of windings and various materials and material combinations. **Figure 1a** illustrates the simple fabrication process starting by dip (spin)-coating of the FC polymer layer onto a Si (glass, flexible) substrate. After heating at 120 °C for 2 min to improve the adhesion of the FC layer on the substrate, we deposit the strained bilayer (multilayer) by electron beam evaporation at a low temperature (<60 °C). The low-temperature deposition is crucial to prevent formation of (micro) cracks caused by thermal stress arising from large temperature changes. After deposition, we heat the samples on a hotplate up to temperatures between 140 and 160 °C. This process step initiates the detachment of the layered nanomembrane from the FC polymer layer and curls the nanomembrane into a compact

microtubular structure (Mechanism I). Similarly, the FC layer can detach from the substrate and partially or totally curl up together with the layered nanomembrane (Mechanism II).

In **Figure 1b**, scanning electron microscopy (SEM) shows the top-view image of long rolled-up microtubes created by the dry FC-assisted rolling process based on mechanism I. The bilayered Ti/Cr (15 nm/20 nm) nanomembrane detaches from the FC polymer layer (thickness: ≈0.2 μm) on the Si substrate and rolls up into microtubes with diameters of ≈11 μm simply upon heating the sample at 140 °C for around ≈5 min. During heating the FC polymer layer experiences more expansion than the metallic nanomembrane because of the much larger coefficient thermal expansion (fluorocarbon polymer (PTFE): >124 × 10⁻⁶ K⁻¹ (25–100 °C),^[20] titanium: 8.4–8.6 × 10⁻⁶ K⁻¹, and chromium: 4.9–8.2 × 10⁻⁶ K⁻¹ (25–100 °C)^[21]). The thermal misfit strain ϵ_{th} between the two constituents, the FC polymeric and metallic bilayer, during high temperature annealing can be expressed as^[18a]

$$\epsilon_{th} = -\Delta\alpha\Delta T = (\alpha_{FC} - \alpha_f)(T_A - T_0) \quad (1)$$

where α_{FC} and α_f are the thermal expansion coefficients of the FC polymer layer and the metal bilayer, respectively, T_A is the annealing (rolling) temperature, and T_0 is the initial temperature which in this case is assumed to be room temperature. The rolling speed is influenced by the amount of thermal strain generated during the heating step. The induced thermal strain and consequently the rolling speed can be controlled by the thickness of the FC polymeric layer as well as the temperature changes during the annealing step. The dependence of the rolling speed, S_r on the FC layer thickness and the rolling temperature is displayed in **Figure 1c,d**. Based on Equation (1) the thermal strain is influenced by the CTE of the FC polymer layer and the inorganic strained bilayer as well as the rolling temperature. It has been shown that the CTE of fluorocarbon polymer (PTFE) thin films is strongly thickness dependent. A model for the thickness dependence of CTE of PTFE by considering both the free surface and the substrate effect has been introduced by Kim and Shi as^[22]

$$\alpha_t / \alpha_\infty = \left\{ \frac{1}{2} \left[\exp\left(\frac{1-a}{t/t_0 - 1}\right) + \exp\left(\frac{1-b}{t/t_0 - 1}\right) \right] \right\}^{-1} \quad (2)$$

where α_t and α_∞ denote the thickness-dependent CTE and the bulk value, respectively, a is a measure of the mobility between polymer and substrate, the mobility near free surface is represented by b , and t_0 represents a characteristic thickness. These parameters, which are dependent to the temperature, are determined by the best fit of the experimental data of the thickness-dependent CTE to Equation (2). Based on their findings, if the segmental mobility of the polymer/substrate is dominant ($a \ll b$), CTE decreases with increasing film thickness (25 and 105 °C). On the other hand, at high temperatures (205 and 305 °C) when the mobility of the polymer near the surface is enhanced and the free surface effect is dominant ($a \gg b$), CTE increases with increasing film thickness.

Substituting Equation (2) into the thermal strain Equation (1) yields the thermal misfit strain as a function of the polymer layer thickness. The thickness dependence of the thermal misfit strain at temperatures of 105 and 205 °C is displayed as “blue”

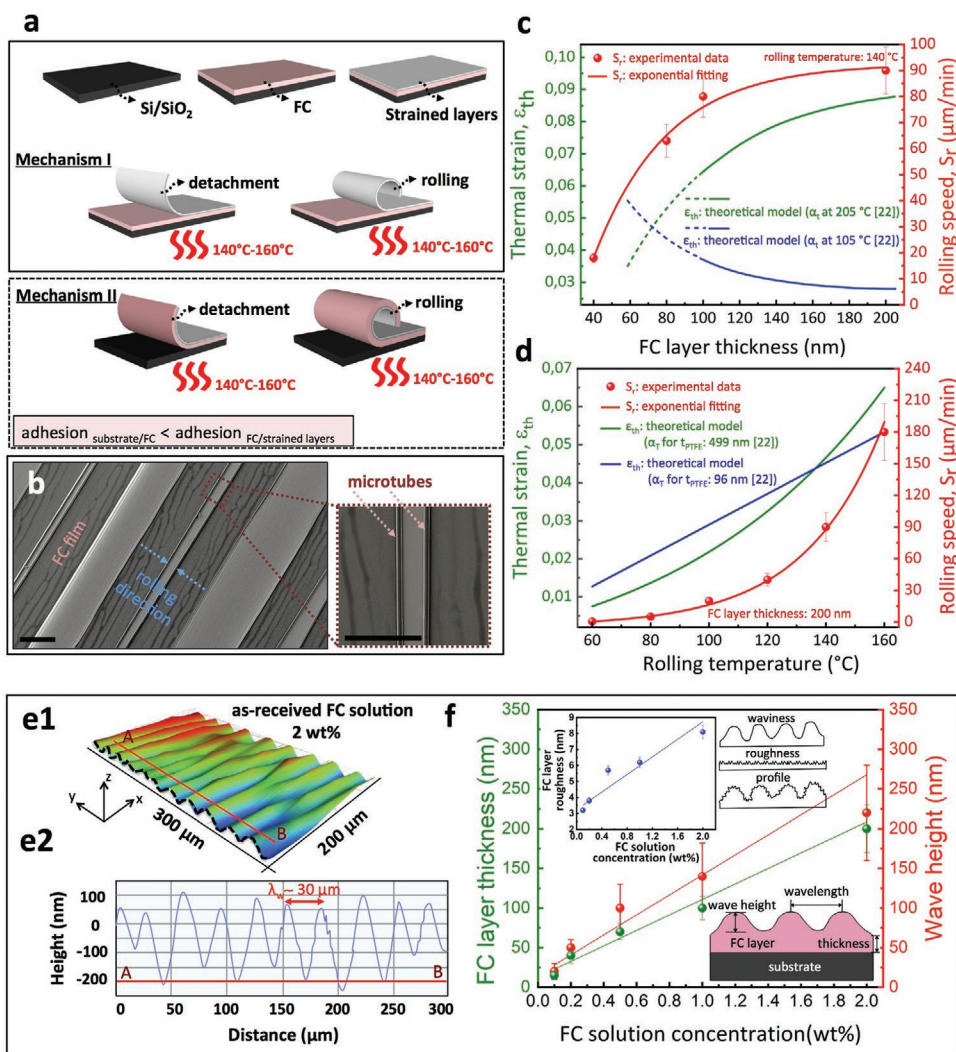


Figure 1. Dry fluorocarbon (FC) layer-assisted and heat-induced rolling technique. a) Schematic illustration of the dry rolling process by means of a FC thin layer upon thermal treatment. Fabrication starting with dip (spin) coating of FC thin layer on a silicon (glass or flexible) substrate as an antistiction layer, following by the strained nanomembrane deposition and eventually detachment of the nanomembrane from FC layer and the rolling process by heat treatment on a hotplate (mechanism I). In the case of lower adhesion between FC layer and substrate compared to nanomembrane and FC layer, the polymer layer also rolls up and is integrated into the windings (mechanism II). b) SEM image featuring millimeter long microtubes released by a 0.2 μm-thick FC layer. Microtubes are comprised of metallic bilayer of Ti/Cr, which detached upon heating at 140 °C. Scale bars are 200 μm. c,d) Dependency of the thermal strain and rolling speed on thickness of FC polymer layer and rolling temperature, respectively. Experimental data are based on strained bilayer comprising Ti/Cr. e1) 3D surface profile of a FC layer dip-coated from an as-received FC solution with concentration of 2 wt% showing waviness profile of the layer surface. e2) 2D line profile displays wave height and wavelength of FC way layer corresponding to AB line shown in 3D profile. f) FC layer thickness, wave height, and roughness as function of FC solution concentration.

and “green” curves, respectively, in Figure 1c. Compared to the blue curve, which does not agree with the rolling manner of our layer system, the green curve nicely reproduces the behavior of the rolling speed, implying that the rolling speed is directly proportional to the thermal misfit strain between the inorganic and the polymer layer. The graph in Figure 1c shows a significant increase in the rolling speed from around ≈ 20 to ≈ 80 μm min⁻¹ when the FC layer thickness increases from ≈ 40 to ≈ 100 nm. This increase is attributed to the strong dependence of the CTE of the polymeric FC layer on the thickness. By increasing CTE of the FC polymer layer, a larger CTE mismatch between the FC layer and the bilayered nanomembrane and consequently a larger thermal stress is introduced in the films upon heating.

For thicker FC layers (>100 nm), the releasing speed saturates and stays independent of the FC layer thickness as the properties of the FC layer are dominated by their bulk material values.

To evaluate the behavior of S_r on the rolling temperature, not only the temperature change during the thermal treatment has to be considered but also the CTE change of the FC layer over the specific temperature range has to be taken into account. Kim and Shi have shown the dependence of the normalized CTE of the FC polymer (PTFE) thin layers on the temperature can be described by a polynomial expression over a specific temperature range^[22]

$$\alpha_T = \alpha_0 + cT \left[1 - \left(\frac{T_0}{T} \right)^2 \right] \quad (3)$$

where α_T is the temperature-dependent CTE, α_0 is CTE at room temperature, c is a constant value which is determined by fitting the experimental data, and T_0 represents room temperature. Based on the analysis of the normalized CTEs of the PTFE samples with different initial thicknesses of 96, 499, and 1154 nm over a specific temperature range they found CTE is nearly independent of the temperature for the thin PTFE polymer layer (96 nm), but for the thick PTFE samples (499 and 1154 nm) is temperature-dependent.

By combining the thermal strain Equations (1) and (3) for the temperature-dependent CTE of the PTFE polymer (499 nm) we obtain the “green” curve plotted in Figure 1d which reproduces the nonlinear behavior of the rolling speed as a function of temperature. By contrast, the “blue” curve which shows a linear relationship between the misfit thermal strain and temperature for the thin PTFE sample (96 nm) does not agree with the rolling speed behavior of the layer system. For the sake of simplicity and because the CTE change over the temperature range of 25–160 °C for the inorganic layers such as Ti and Cr is very low ($<2 \times 10^{-6} \text{ K}^{-1}$)^[23] compared to the PTFE polymeric layer ($\approx 250 \times 10^{-6} \text{ K}^{-1}$ for 500 nm-thick PTFE),^[22] we consider that the CTE value of the inorganic strained bilayer is independent of the temperature. The rolling speed ($\approx 5 \text{ } \mu\text{m min}^{-1}$) is lowest at a temperature just below 80 °C slightly increasing when the temperature rises to 120 °C. The CTE mismatch increases as the annealing temperature rises, which in turn causes a continuous increase in the misfit thermal strain and consequently the rolling speed.

Investigating the surface morphology of the FC layer is crucial to understand the details of the fabrication method and to achieve optimized tube configurations. Figure 1e1 reveals the 3D surface profile of a dip-coated FC layer showing a wavy profile of the layer surface. The 2D line scan given in Figure 1e2 provides the wave height amplitude ($220 \pm 60 \text{ nm}$) and wavelength ($30 \pm 5 \text{ } \mu\text{m}$) of the pattern. As shown in Figure 1f, the FC layer thickness, wave height, and roughness, which strongly affect the tightness level of the microtube windings, can be tuned by dilution of the FC solution. Diluting the FC solution in fluorocarbon-based solvent from 2 to 0.1 wt% causes the FC layer thickness and wave height to decrease from ≈ 200 to $\approx 15 \text{ nm}$ and from ≈ 220 to $\approx 20 \text{ nm}$, respectively, when the dip-coating process is applied. Similarly, the FC layer roughness is reduced from around ≈ 8.2 to $\approx 3.1 \text{ nm}$ by the same dilution factor.

To demonstrate the ability of the proposed approach to create highly symmetric and ultracompact multiwinding microtubes, we carried out a comprehensive investigation of the cross-sectional structure of the fabricated microtubes by focused ion beam (FIB) preparation and scanning electron microscopy (SEM). **Figure 2a** shows cross-sectional SEM images of a highly compact multiple winding microtube consisting of alternating layers of Ti (15 nm)/Cr (20 nm)/Al₂O₃ (11 nm)/Cr (30 nm)/Al₂O₃ (11 nm). The rolling process was done using a thin FC layer with a thickness of $\approx 40 \text{ nm}$ (FC solution concentration: 0.2 wt%) upon heating at 140 °C. The image of a void-less rolled-up microtube with 13 windings demonstrates the capability of the dry method to create structurally perfect ultracompact multiwinding tubular structures. The extra thermal stress in combination with the intrinsic strain gradient in the layered

nanomembrane provides a large driving force for the roll-up upon thermal treatment at high temperatures. The dry nature of the technique, which excludes any fluids to enter neighboring windings and the smooth delamination of the nanomembrane by means of the hydrophobic polymer layer are responsible for providing defect-free interfaces of the alternating layers in the microtube structure. From the magnified cross-sectional SEM in Figure 2a3 we find that the rolling process was governed by mechanism II as the FC layer was entirely rolled up together with the metal and oxide nanomembrane. Another cross-sectional image of a rolled-up microtube with an even higher number of windings is shown in Figure 2b. The microtube consists of a bilayered nanomembrane of Ti (15 nm)/Cr (20 nm) with around 50 tight windings and an average outer diameter of $\approx 7 \text{ } \mu\text{m}$. Similarly, the rolling process was done using a thin FC layer with a thickness of $\approx 40 \text{ nm}$. In the magnified cross-sectional SEM image in Figure 2b3, this FC thin layer can again be detected in the windings.

One factor that controls the mechanism of the rolling process is the thickness of the FC layer. For large FC layer thicknesses (normally above 100 nm), the rolling process is governed by mechanism I. However, as the thickness of the FC layer decreases to values around 50 nm and less mechanism II becomes dominant. In this case, applying thermal treatment or using adhesion promoter materials to improve the adhesion of the FC layer to the substrate can prevent the FC layer to roll up. One explanation for why the FC layer thickness can control the nature of the rolling mechanism is the effect of certain FC layer morphological features (waviness and roughness) on the wettability of the FC layer that is dependent on the thickness of the FC layer. The relationship between the surface roughness and wettability of solid surfaces has been described by the well-known Wenzel model which implies that surface roughness always amplifies the wetting properties of a given surface.^[24] Therefore, a surface roughness renders hydrophobic surfaces even more hydrophobic. The effect of surface morphology on the wettability of the FC polymer surfaces as extreme hydrophobic polymers has been reported by several research works and the results have shown that even extremely low surface roughness values (nanometer range) are important and influence the wetting behavior of these polymers.^[25] It has also been realized that by micro- and nanotexturing a FC polymer surface to increase its roughness, the wettability can be decreased.^[26] According to our investigation on the effect of the rolling temperature on the rolling mechanism, we did not observe any significant change in the rolling mechanism at different temperatures. Therefore, we assume a thickness-dependent adhesion between the FC layer and the strained nanomembrane rather than a temperature-dependent adhesion. Moreover, it is reasonable to assume that the detachment of a thick polymeric layer is more difficult compared to a thinner layer of the same strained nanomembrane and adhesion condition. Different approaches to determine the mechanism type of the rolling process in the dry FC-assisted rolling technique have been presented in detail in Figures S1 and S2 (Supporting Information).

We confirmed that the tightness of the windings is not limited to particular parts along the axis of the microtube. This is especially important for tubular devices, in, e.g., optical applications,^[7e,27] where the light needs to propagate along the

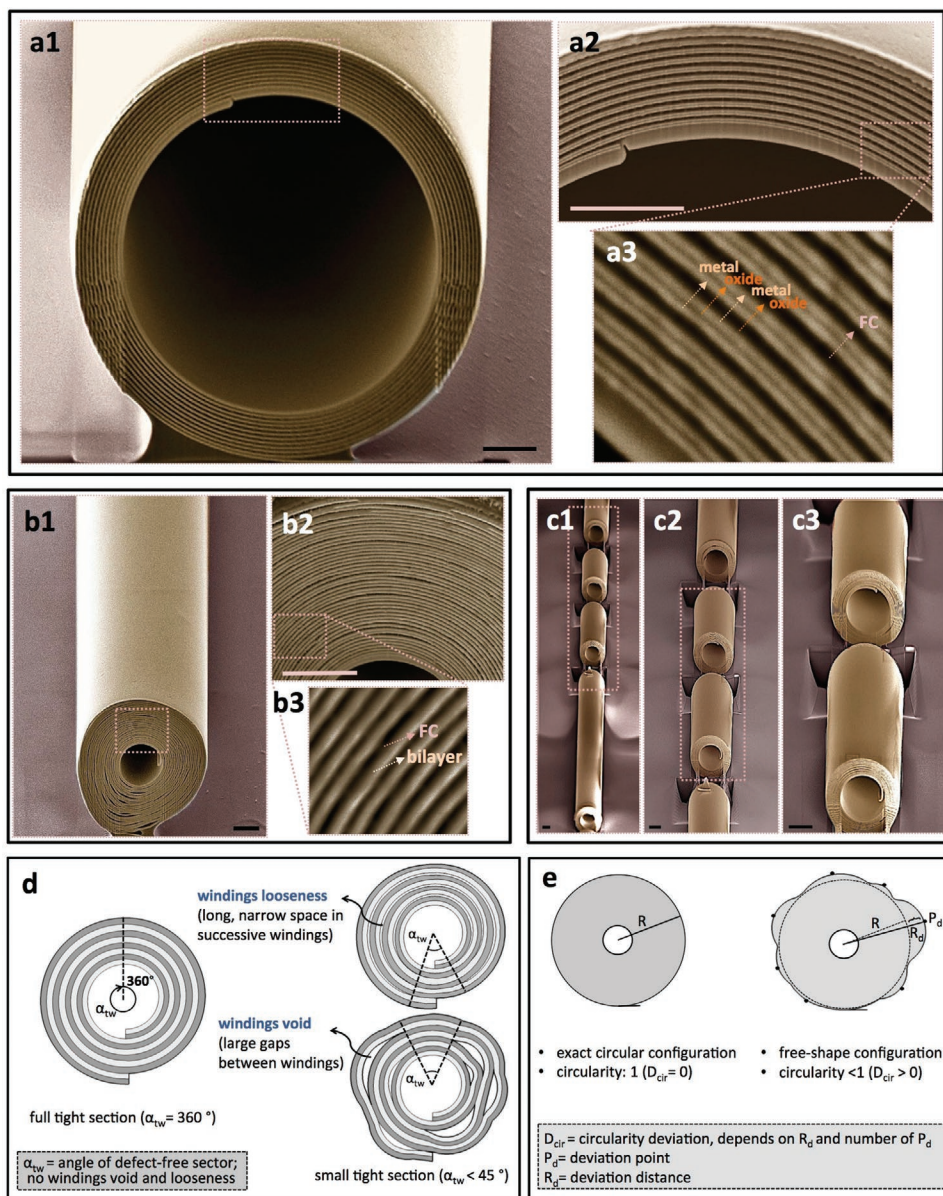


Figure 2. Structural characterization of multiple winding rolled-up microtubes fabricated by dry FC-assisted rolling approach. a–c) False-colored cross-section SEM images of the rolled-up microtubes made from different material combinations and winding numbers. a1) Symmetric and tight rolled-up microtube consisting of Ti/Cr/Al₂O₃/Cr/Al₂O₃ layers and 13 rotations. a2,3) Magnified SEM images revealing consecutive layers of metal and oxide separated by a thin FC layer. b1) Rolled-up Ti/Cr microtube consisting of about 50 tightly wrapped windings. b2,3) Magnified SEM images of bilayered rolled-up microtube. c) Microtube made of Ti/Au/TiO₂/Cr layers with several FIB cuts at different positions proving tightness of the windings along the whole length of the microtube. d,e) Quantitative structural analysis of all rolled-up tubular structures: d) rolled-up microtube defect-free sector angle, α_w and e) microtube shape circularity. Scale bars are 2 μ m. Scale bars in (a3) and (b3) are 100 nm.

whole length of the microtube. To explore this critical feature, we prepared several FIB cuts at different positions along the axis of the microtube. Figure 2c shows cross-sectional images of a long microtube thermally rolled up from a multilayer nanomembrane consisting of Ti (10 nm)/Au (10 nm)/TiO₂ (25 nm)/Cr (15 nm) which was cut into several fragments of different lengths ranging from around \approx 20 to \approx 60 μ m.

In the following, we present a comprehensive quantitative structural analysis of the rolled-up microtubular components. The precise structural analysis is an essential part in rolled-up

nanotechnology as any imperfection in the layer structure of a rolled-up device can directly influence its main functionalities. To do this, we carefully define certain quality parameters, which are essential to be fulfilled by a high quality multi-winding microtube. As schematically depicted in Figure 2d, one key parameter of a multiwinding rolled-up microtube is the angle of a sector (α_w) in which tight windings free of interfacial defects (including winding void (large gap) or winding looseness (continuously long narrow space)) can be found. Based on this definition, a perfectly wound microtube has a value of

$\alpha_{tw} = 360^\circ$. Apart from the absolute number of void and looseness in consecutive windings, the distribution pattern of the interfacial defects over the cross section can influence this angle. Another important factor that can crucially affect the performance of rolled-up devices, especially those that are sensitive to the geometric shape, such as high frequency electronics and optics,^[28] is the degree of symmetry (circularity) of a rolled-up microtube. As illustrated in Figure 2e, the deviation from circularity can be defined by the normalized average distance from the surface points to the nearest points on a perfect circle. The deviation from circular symmetry is greatly influenced by the number, scale and even the distribution pattern of the interface defects between the windings. While for an exact circular shape the circularity value is defined as one, by increasing the circularity deviation, the circularity value decreases. The dependence of these two factors on FC layer morphology has been thoroughly investigated and is presented in Figure S3 (Supporting Information).

The uniqueness of the heat activation rolling approach is the capability of creating rolled-up multiwinding microtubes with a high degree of compactness independent of the number of rotations. Figure 3a presents microtubes with different number of windings using a strained multilayer nanomembrane comprising Ti (10 nm)/Au (10 nm)/TiO₂ (25 nm)/Cr (15 nm) released together with an ≈ 40 nm thick FC layer at 160 °C. Figure 3a1–3 shows the cross-section SEM images of the microtubes with 8, 15, and 50 windings, respectively. The microtubes are free from extended voids between the windings even in the case of the microtube with ≈ 50 windings. Energy-dispersive X-ray (EDX) analysis at different positions on the sample including the rolled part, tube surface, and unrolled part of the nanomembrane displayed in Figure 3b, indicates that the FC layer is also found in the microtube together with the metal and oxide layers.

To quantitatively compare the structural perfection of the rolled-up microtubes fabricated by the dry FC-assisted rolling technique with conventional wet chemical etching methods, we conducted a thorough study based on tightness angle and circularity degree derived from cross-sectional images presented in previous publications^[7a,9a,11b,14a,27a,28b,29] and our own experimental data (details of the wet chemistry rolling process are given in the Experimental Section). The results of this analysis are plotted in Figure 3c and reveal that by employing the dry FC-assisted rolling technique the tightness angle experiences a slight decrease from $\approx 360^\circ$ to $\approx 270^\circ$ when the number of windings increases from around 2 to 50. In contrast, applying conventional wet chemistry causes the tightness angle to drop quickly and reach a value of $\approx 60^\circ$ when the rotation number increases to only 10. The dependence of circularity on the winding number for microtubes fabricated by these two different methods (dry and wet) is depicted in the figure as well. The number of microtube windings has a direct impact on the quality of the cylindrical shape for microtubes produced by wet chemistry. While it is not difficult to achieve high circularity for a microtube with a few windings (<3), it becomes increasingly more difficult to achieve a round shape for larger winding numbers (>10).

Similar to the continuous strained nanomembranes which can be rolled to create highly compact multiwinding microtubes, rolling of the patterned strained nanomembrane

(photolithography process) in a well-controlled unidirectional manner (angled deposition process^[14a,30]) can be managed by this technique as well. In both cases, a high yield (>90%) of the extremely compact multiwinding microtubes was obtained by applying the optimized rolling conditions such as using thin FC layers (thickness ≤ 40 nm). Moreover, by applying angled deposition, we could force the patterned strained nanomembranes to exhibit unidirectional rolling with a yield of 40% to 70% depending on the pattern shape, dimensions and tilt angle of the angled deposition process. The compatibility of the FC-assisted rolling technique with optical lithography is discussed in detail in Supporting Information (Figures S4–S6, Supporting Information).

Tightly packed windings fabricated by dry rolling significantly enhance the mechanical stability of the microtubes. This opens up the possibility to reliably produce entirely freestanding microtubes where a large part of the microtube extends over the substrate edge.^[1b] Fabricating such freestanding microtubes constitutes a promising way to eliminate the frustrating and time-consuming transferring process^[31] when microtubular devices need to be aligned with measurement setups. Moreover, such entirely freestanding microtube sections may provide perfect conditions to accurately measure the microtube structural performance without interfering with the substrate surface. Figure 3d1,2 shows SEM images of the freestanding microtubes with different free part lengths (L_{fp}) as defined in Figure 3d3. The microtube shown in Figure 3d2 consists of ≈ 50 windings with a 2.5 mm long free part. Figure S7 (Supporting Information) shows details of the fabrication process.

Tailoring the wrinkling (buckling) phenomenon^[16d,32,33] in combination with the strain-engineering rolled-up nanotechnology and the novel dry rolling platform enables us to introduce a methodology to produce rolled-up structures with aligned wrinkling patterns. On a flat underlayer surface, there is neither a preferred orientation for the wrinkles, nor a reason for the wrinkles to form systematic patterns, thus the film wrinkles are randomly disordered.^[32,34,35] However, on a nonflat surface having a bas-relief pattern such as the wavy surface of the FC layer, the stress in the film is not uniform, instead, there is a strong orientation of the stress in the vicinity of the relief structures.^[35] Therefore, the wrinkles form in patterns ordered near the FC layer waves as the relief features. Depending on the waviness level of the FC polymeric layer, microtubes decorated with different wrinkling patterns are easily fabricated and displayed in Figure 3e1–5. These hierarchical well-ordered wrinkled microtubes may open up new avenues in the future interdisciplinary field of rolled-up nanotechnology. The mechanism for the formation of these fascinating structures is presented in Figure S8 (Supporting Information).

In summary, we introduced a dry rolling technique exploiting the hydrophobicity feature of a polymeric release layer together with the thermal expansion mismatch of the polymers and inorganic films upon thermal treatment. This approach enables rolled-up nanotechnology to create highly symmetric and compact multi-winding microtubes. A systematic structural analysis allows us to define quality parameters against which we benchmark rolled up microtubes produced by different technologies (e.g., wet and dry etching). The high mechanical stability of

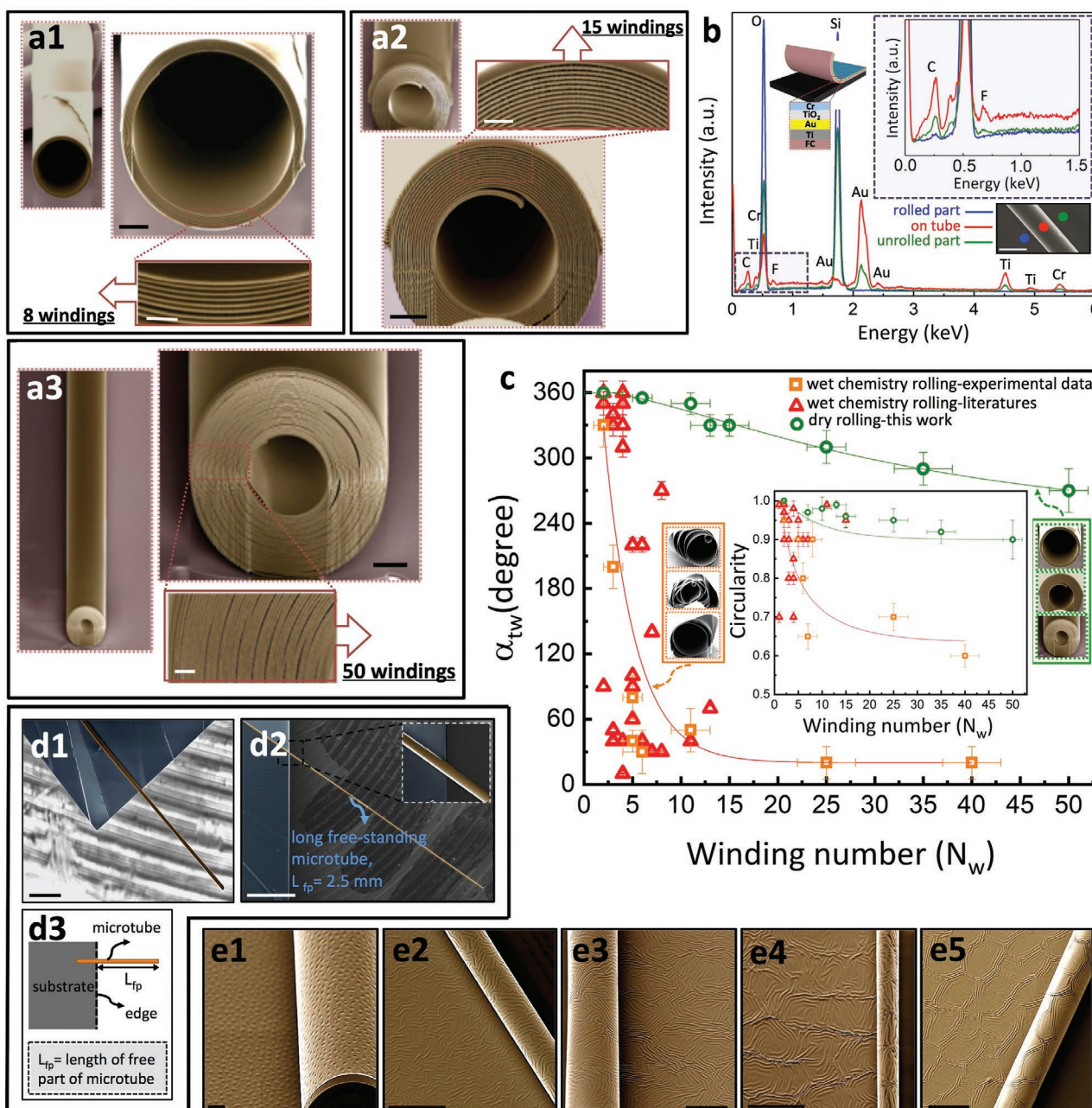


Figure 3. Compact multiwall rolled-up microtubes, capability of engineering freestanding microtubes and ability of decorating microtubes with aligned wrinkling patterns. a1–3) False-colored cross-sectional SEM images of microtubes comprising Ti/Au/TiO₂/Cr layers and different winding numbers (8, 15, and 50). Scale bars in full cross-section SEM images represent 2 μ m. Scale bars of magnified SEM images are 500 nm. b) Energy-dispersive X-ray spectrum analysis of the microtubes displayed in (a1)–(a3). Scale bar of inset image is 10 μ m. c) Microtube tightness angle (α_{tw}) and circularity as function of winding number of rolled-up microtubes. All measurement data are based on the cross-section images of the microtubes released from a thin FC layer (≈ 40 nm). d1) False-colored SEM image of a single freestanding microtube. d2) False-colored SEM image of a freestanding microtube with a free part length, L_{fp} of around ≈ 2.5 mm. d3) Schematic illustration of a freestanding microtube. Microtubes presented in (d1) and (d2) consist of Ti/Cr bilayer nanomembranes. Scale bars in (d1) and (d2) are 100 and 500 μ m, respectively. e1–5) False-colored SEM images of different wrinkling patterns rolled-up into microtubes. Surface wrinkling patterns are changed by waviness level of FC release layer, which is dependent on FC solution concentration. FC wavy layers made of different solution concentrations (0.1, 0.2, 0.5, 1, 2 wt%). All microtubes presented in (e1)–(e5) are made of Ti/Au/Cr layers and scale bars are 10 μ m.

compact multiwound microtubes will help to ensure reliable integration into technological applications. The dry rolling technique provides ordered wrinkle patterns which can be integrated into the hierarchical structure of microtubes after the roll-up

process. Our work opens up possibilities toward realizing highly complex device architectures such as metamaterial optical fibers or cylindrical photonic crystals, which have been out of reach by traditional wet chemical etching technologies.

Experimental Section

FC Release Layer Preparation: First, the substrate was sonicated by immersing in DMSO, acetone, and isopropanol for 3 min and subsequently followed by O₂ plasma etching step to remove any residuals from the substrate surface. After cleaning, the antistiction FC layer using a commercially available fluoropolymers solution (3M Novec 1700 Electronic Grade Coating), which is a clear, low viscosity solution of a 2 wt% fluorochemical acrylic polymer carried in a hydrofluoroether solvent was dip (spin) coated on the substrate. Afterward, sample was annealed at 100 °C for 1 min to remove all the solvent residuals. Various concentrations of FC solution (0.1–2 wt%) can be prepared using a fluorocarbon-based solvent (3M Novec Engineered Fluid 7100).

Deposition of the Strained Layers on FC Layer: Deposition of the strained metal layers including Ti, Cr, and Au was done in a conventional e-beam evaporator (IM9912-Micronova) under high vacuum (<10⁻⁶ mbar). Precisely controlling the sample temperature during the deposition process is crucial to prevent initiation and propagation of the (micro) cracks. The maximum temperature, which the samples could tolerate without any crack formation was 60 °C. In order to guarantee the constant low temperature condition during the metal evaporation process, a sample holder with large distance from the materials crucible (290 mm) was installed. To provide enough intrinsic strain induced by the deposition process in this larger distance, the deposition rates of 2.5, 3, and 2 Å s⁻¹ for Ti, Cr, and Au, were set, respectively. The oxide layers such as Al₂O₃ and TiO₂ were deposited by atomic layer deposition (ALD) (Savannah 100, Cambridge NanoTech Inc.). Al₂O₃ layers were deposited at 80 °C (1.1 Å cycle⁻¹), while TiO₂ layers were deposited at 160 °C (0.5 Å cycle⁻¹).

Wet Chemistry Rolling Process: The 20 nm LiPON as the sacrificial layer was deposited via reactive sputtering deposition (Moorfield MiniLab 60) using a Li₃PO₄ target (Evochem) in nitrogen atmosphere. Immediately after deposition the sacrificial layer was covered by a thin layer of Al₂O₃ (11 nm) to protect it from dissolution in the air humidity and aqueous solutions during photolithography steps. Afterward, different strained nanomembranes including a trimetallic nanomembrane consisting of Au (5 nm)/Ti (15 nm)/Cr (20 nm) and a multilayer nanomembrane made of Au (5 nm)/Ti (15 nm)/Cr (20 nm)/Al₂O₃ (11 nm)/Cr (30 nm) were deposited on top of the oxide layer. The Au, Ti, and Cr layers were deposited via electron-beam evaporation (IM9912-Micronova) with the rates of 1, 1, and 3 Å s⁻¹, respectively. The oxide layer was grown by ALD (SavannahTM 100, Cambridge NanoTech Inc.) at 200 °C with a rate of 1.1 Å cycle⁻¹. For releasing the nanomembrane, the substrate was immersed in deionized water (DI) as the wet etchant solution at 70 °C to start selectively removing the sacrificial layer and rolling up the nanomembrane.

Morphology Characterization of FC Release Layer: Morphology investigation of FC layers including surface roughness, thickness, and wave height measurements was done by using Stylus Profilometer (Veeco Dektak-8) and atomic force microscopy (AFM) (Agilent 5600LS system) under an argon controlled environment. AFM measurements were performed in tapping mode using special ultrasharp (4–10 nm tip radius) Olympus cantilevers, which allowed high-resolution measurements. 3D surface mapping of FC layer was done by a Dektak XT stylus profiler (Bruker).

Microtubes Cross-Sectional Characterization: Fabricated microtubes were imaged using a scanning electron microscopy (NVision 40 CrossBeam, Carl Zeiss). Images were obtained using the acceleration voltage of 2–5 kV. The cross-sectional images of the microtubes in order to investigate quality of the windings interface were prepared by an attached Ga-ion FIB milling column for vertical cutting (Zeiss NVision40 dual-beam). Energy-dispersive X-ray spectroscopy analysis for the elemental analysis of the microtubes was carried out using a SEM Ultra Plus with an attached peltier cooled Si(Li) detector (Oxford instruments).

Microtube Circularity Calculation: The outer shape circularity was measured on the cross-sectional images of the rolled-up microtubes using image analysis software “ImageJ.”

Supporting Information

Supporting Information is available from the Wiley Online Library or from the author.

Acknowledgements

The authors thank Paul Plocica, Eric Pankenin, Martin Bauer, Stephan Rölz, and Stefan Baunack for the technical support and helpful discussions. This work was financed by the International Research Training Group (IRTG) project GRK 1215 “Materials and Concepts for Advanced Interconnects and Nanosystems.” V.K.B. acknowledges the support and funding from the European Social Fund (ESF). O.G.S. acknowledges financial support by the Leibniz Program of the German Research Foundation (SCHM 1298/26-1).

Conflict of Interest

The authors declare no conflict of interest.

Keywords

dry rolling, fluorocarbon polymers, microtube windings compactness, rolled-up technology, thermal treatment

Received: December 5, 2019

Revised: March 17, 2020

Published online: May 11, 2020

- [1] a) O. G. Schmidt, K. Eberl, *Nature* **2001**, *410*, 168; b) V. Y. Prinz, V. A. Seleznev, A. K. Gutakovskiy, A. V. Chehovskiy, V. V. Preobrazhenskii, M. A. Putyato, T. A. Gavrilova, *Phys. E* **2000**, *6*, 828; c) O. G. Schmidt, N. Schmarje, C. Deneke, C. Müller, N. Y. Jin-Phillipp, *Adv. Mater.* **2001**, *13*, 756; d) G. Huang, Y. Mei, D. J. Thurmer, E. Coric, O. G. Schmidt, *Lab Chip* **2009**, *9*, 263; e) Y. Yin, T. Qiu, L. Ma, X. Lang, Y. Zhang, G. Huang, Y. Mei, O. G. Schmidt, *J. Phys. Chem. C* **2012**, *116*, 25504; f) D. Karnaushenko, T. Kang, O. G. Schmidt, *Adv. Mater. Technol.* **2019**, *4*, 1800692; g) J. Rogers, Y. Huang, O. G. Schmidt, D. H. Gracias, *MRS Bull.* **2016**, *41*, 123.
- [2] D. Grimm, C. C. B. Bufon, C. Deneke, P. Atkinson, D. J. Thurmer, F. Schäffel, S. Gorantla, A. Bachmatiuk, O. G. Schmidt, *Nano Lett.* **2013**, *13*, 213.
- [3] a) A. Bernardi, S. Kiravittaya, A. Rastelli, R. Songmuang, D. J. Thurmer, M. Benyoucef, O. G. Schmidt, *Appl. Phys. Lett.* **2008**, *93*, 094106; b) A. Madani, M. Kleinert, D. Stolarek, L. Zimmermann, L. Ma, O. G. Schmidt, *Opt. Lett.* **2015**, *40*, 3826.
- [4] D. J. Thurmer, C. Deneke, Y. Mei, O. G. Schmidt, *Appl. Phys. Lett.* **2006**, *89*, 223507.
- [5] M. Medina-Sánchez, B. Ibarlucea, N. Pérez, D. D. Karnaushenko, S. M. Weiz, L. Baraban, G. Cuniberti, O. G. Schmidt, *Nano Lett.* **2016**, *16*, 4288.
- [6] R. Streubel, D. J. Thurmer, D. Makarov, F. Kronast, T. Kosub, V. Kravchuk, D. D. Sheka, Y. Gaididei, R. Schäfer, O. G. Schmidt, *Nano Lett.* **2012**, *12*, 3961.
- [7] a) R. Streubel, L. Han, F. Kronast, A. A. Ünal, O. G. Schmidt, D. Makarov, *Nano Lett.* **2014**, *14*, 3981; b) S. Böttner, S. Li, M. R. Jorgensen, O. G. Schmidt, *Appl. Phys. Lett.* **2013**, *102*, 251119; c) A. A. Solovov, Y. Mei, E. Bermúdez-Ureña, G. Huang, O. G. Schmidt, *Small* **2009**, *5*, 1688; d) C. S. Martinez-Cisneros,

- S. Sanchez, W. Xi, O. G. Schmidt, *Nano Lett.* **2014**, *14*, 2219; e) G. Huang, V. A. B. Quiñones, F. Ding, S. Kiravittaya, Y. Mei, O. G. Schmidt, *ACS Nano* **2010**, *4*, 3123.
- [8] a) C. C. B. Bufon, J. D. C. González, D. J. Thurmer, D. Grimm, M. Bauer, O. G. Schmidt, *Nano Lett.* **2010**, *10*, 2506; b) R. Sharma, C. C. B. Bufon, D. Grimm, R. Sommer, A. Wollatz, J. Schadowald, D. J. Thurmer, P. F. Siles, M. Bauer, O. G. Schmidt, *Adv. Energy Mater.* **2014**, *4*, 1301631.
- [9] a) X. Yu, W. Huang, M. Li, T. M. Comberiate, S. Gong, J. E. Schutt-Aine, X. Li, *Sci. Rep.* **2015**, *5*, 9661; b) D. D. Karnausenko, D. Karnausenko, H.-J. Grafe, V. Kataev, B. Büchner, O. G. Schmidt, *Adv. Electron. Mater.* **2018**, *4*, 1800298.
- [10] E. J. Smith, Z. Liu, Y. Mei, O. G. Schmidt, *Nano Lett.* **2010**, *10*, 1.
- [11] a) E. J. Smith, Z. Liu, Y. F. Mei, O. G. Schmidt, *Appl. Phys. Lett.* **2009**, *95*, 083104; b) S. Schwaiger, A. Rottler, M. Bröll, J. Ehlermann, A. Stemmann, D. Stickler, C. Heyn, D. Heitmann, S. Mendach, *Phys. Rev. B* **2012**, *85*, 235309; c) S. Schwaiger, A. Rottler, S. Mendach, *Adv. Optoelectron.* **2012**, *2012*, 782864; d) G. Brumfiel, *Nature* **2009**, *459*, 504.
- [12] M. R. Jorgensen, S. Giudicatti, O. G. Schmidt, *Phys. Rev. A* **2013**, *87*, 041803.
- [13] R. M. Costescu, C. Deneke, D. J. Thurmer, O. G. Schmidt, *Nanoscale Res. Lett.* **2009**, *4*, 1463.
- [14] a) Y. Mei, G. Huang, A. A. Solovev, E. B. Ureña, I. Mönch, F. Ding, T. Reindl, R. K. Y. Fu, P. K. Chu, O. G. Schmidt, *Adv. Mater.* **2008**, *20*, 4085; b) E. J. Smith, D. Makarov, O. G. Schmidt, *Soft Matter* **2011**, *7*, 11309.
- [15] a) J. Li, J. Zhang, W. Gao, G. Huang, Z. Di, R. Liu, J. Wang, Y. Mei, *Adv. Mater.* **2013**, *25*, 3715; b) F. Ma, B. Xu, S. Wu, L. Wang, B. Zhang, G. Huang, A. Du, B. Zhou, Y. Mei, *Nanotechnology* **2019**, *30*, 354001.
- [16] a) M. George, C. Coupeau, J. Colin, F. Cleymand, J. Grilhé, *Philos. Mag. A* **2002**, *82*, 633; b) H. Yu, J. W. Hutchinson, *Thin Solid Films* **2003**, *423*, 54; c) Z. Jia, C. Peng, J. Lou, T. Li, *Thin Solid Films* **2012**, *520*, 6576; d) J. Lewis, *Mater. Today* **2006**, *9*, 38.
- [17] V. K. Khanna, *J. Phys. D: Appl. Phys.* **2011**, *44*, 034004.
- [18] a) M. F. Doerner, W. D. Nix, *Crit. Rev. Solid State Mater. Sci.* **1988**, *14*, 225; b) W. Fang, C. Lo, *Sens. Actuators, A* **2000**, *84*, 310; c) D. Khang, H. Jiang, Y. Huang, J. A. Rogers, *Science* **2006**, *311*, 208.
- [19] a) H. V. Jansen, J. G. E. Gardeniers, J. Elders, H. A. C. Tilmans, M. Elwenspoek, *Sens. Actuators, A* **1994**, *41*, 136; b) D. Haefliger, M. Nordström, P. A. Rasmussen, A. Boisen, *Microelectron. Eng.* **2005**, *78*, 88; c) B. K. Smith, J. J. Sniogowski, G. LaVigne, C. Brown, *Sens. Actuators, A* **1998**, *70*, 159.
- [20] R. K. Kirby, *J. Res. Natl. Bur. Stand.* **1956**, *57*, 91.
- [21] ASM International Materials Properties Database Committee, *ASM Ready Reference: Thermal Properties of Metals*, ASM International, Materials Park, OH **2002**.
- [22] H. Kim, F. G. Shi, in *IEEE 52nd Electronic Components and Technology Conf.*, San Diego, CA **2002**, p. 1581.
- [23] a) Z. Nibennaoune, D. George, S. Ahzi, D. Ruch, Y. Remond, J. J. Gracio, *Thin Solid Films* **2010**, *518*, 3260; b) G. Laplanche, P. Gadaud, C. Bärsch, K. Demtröder, C. Reinhart, J. Schreuer, E. P. George, *J. Alloys Compd.* **2018**, *746*, 244.
- [24] R. N. Wenzel, *Ind. Eng. Chem.* **1936**, *28*, 988.
- [25] a) V. Pachchigar, M. Ranjan, S. Mukherjee, *Sci. Rep.* **2019**, *9*, 8675; b) J. D. Miller, S. Veeramani, J. Drelich, M. R. Yalamanchili, G. Yamauchi, *Polym. Eng. Sci.* **1996**, *36*, 1849; c) J. Ryu, K. Kim, J. Y. Park, B. G. Hwang, Y. C. Ko, H. J. Kim, J. S. Han, E. R. Seo, Y. J. Park, S. J. Lee, *Sci. Rep.* **2017**, *7*, 1981.
- [26] a) G. H. ten Brink, N. Foley, D. Zwaan, B. J. Kooi, G. Palasantzas, *RSC Adv.* **2015**, *5*, 28696; b) L. R. J. Scarratt, B. S. Hoatson, E. S. Wood, B. S. Hawkett, C. Neto, *ACS Appl. Mater. Interfaces* **2016**, *8*, 6743; c) Y. Rane, A. Altecort, N. S. Bell, K. Lozano, *J. Eng. Fibers Fabr.* **2013**, *8*, 88.
- [27] a) R. Songmuang, A. Rastelli, S. Mendach, O. G. Schmidt, *Appl. Phys. Lett.* **2007**, *90*, 091905; b) U. Vogl, A. Saß, F. Vewinger, M. Weitz, A. Solovev, Y. Mei, O. G. Schmidt, *Phys. Rev. A* **2011**, *83*, 053403.
- [28] a) G. S. Huang, S. Kiravittaya, V. A. B. Quiñones, F. Ding, M. Benyoucef, A. Rastelli, Y. F. Mei, O. G. Schmidt, *Appl. Phys. Lett.* **2009**, *94*, 141901; b) G. S. Huang, Y. F. Mei, F. Cavallo, S. Baunack, E. Coric, T. Gemming, F. Bertram, J. Christen, R. K. Y. Fu, P. K. Chu, O. G. Schmidt, *J. Appl. Phys.* **2009**, *105*, 016103.
- [29] a) R. Songmuang, A. Rastelli, S. Mendach, C. Deneke, O. G. Schmidt, *Microelectron. Eng.* **2007**, *84*, 1427; b) F. Cavallo, W. Sigle, O. G. Schmidt, *J. Appl. Phys.* **2008**, *103*, 116103; c) C. Müller, G. B. de Souza, A. Mikowski, O. G. Schmidt, C. M. Lepienski, D. H. Mosca, *J. Appl. Phys.* **2011**, *110*, 044326; d) C. Müller, C. C. B. Bufon, M. E. N. Fuentes, D. Makarov, D. H. Mosca, O. G. Schmidt, *Appl. Phys. Lett.* **2012**, *100*, 022409; e) A. Malachias, Ch. Deneke, B. Krause, C. Mocuta, S. Kiravittaya, T. H. Metzger, O. G. Schmidt, *Phys. Rev. B* **2009**, *79*, 035301; f) H. Ji, X. Wu, L. Fan, C. Krien, I. Fiering, Y. Guo, Y. Mei, O. G. Schmidt, *Adv. Mater.* **2010**, *22*, 4591; g) L. Zhang, J. Deng, L. Liu, W. Si, S. Oswald, L. Xi, M. Kundu, G. Ma, T. Gemming, S. Baunack, F. Ding, C. Yan, O. G. Schmidt, *Adv. Mater.* **2014**, *26*, 4527; h) X. Lu, J. Deng, W. Si, X. Sun, X. Liu, B. Liu, L. Liu, S. Oswald, S. Baunack, H. J. Grafe, C. Yan, O. G. Schmidt, *Adv. Sci.* **2015**, *2*, 1500113; i) G. Li, M. Yarali, A. Cocemasov, S. Baunack, D. L. Nika, V. M. Fomin, S. Singh, T. Gemming, F. Zhu, A. Mavrokefalos, O. G. Schmidt, *ACS Nano* **2017**, *11*, 8215; j) E. Bermúdez-Ureña, Y. Mei, E. Coric, D. Makarov, M. Albrecht, O. G. Schmidt, *J. Phys. D: Appl. Phys.* **2009**, *42*, 055001; k) C. Müller, C. C. B. Bufon, D. Makarov, L. E. Fernandez-Outon, W. A. A. Macedo, O. G. Schmidt, D. H. Mosca, *Nanoscale* **2012**, *4*, 7155; l) S. Giudicatti, S. M. Marz, L. Soler, A. Madani, M. R. Jorgensen, S. Sanchez, O. G. Schmidt, *J. Mater. Chem. C* **2014**, *2*, 5892; m) A. Madani, L. Ma, S. Miao, M. R. Jorgensen, O. G. Schmidt, *Nanoscale* **2016**, *8*, 9498; n) C. Deneke, R. Songmuang, N. Y. Jin-Phillipp, O. G. Schmidt, *J. Phys. D: Appl. Phys.* **2009**, *42*, 103001; o) S. Giudicatti, S. M. Marz, S. Böttner, B. Eichler, M. R. Jorgensen, O. G. Schmidt, *Proc. SPIE* **2014**, *9127*, 912706.
- [30] Z. Wang, P. R. West, X. Meng, N. Kinsey, V. M. Shalae, A. Boltasseva, *MRS Commun.* **2016**, *6*, 17.
- [31] Z. Tian, F. Li, Z. Mi, D. V. Plant, *IEEE Photonics Technol. Lett.* **2010**, *22*, 311.
- [32] a) F. Cavallo, M. G. Lagally, *Soft Matter* **2010**, *6*, 439; b) Y. Mei, S. Kiravittaya, S. Harazim, O. G. Schmidt, *Mater. Sci. Eng., R* **2010**, *70*, 209.
- [33] P. Cendula, S. Kiravittaya, Y. F. Mei, C. Deneke, O. G. Schmidt, *Phys. Rev. B* **2009**, *79*, 085429.
- [34] C. M. Stafford, S. Guo, C. Harrison, M. Y. M. Chiang, *Rev. Sci. Instrum.* **2005**, *76*, 062207.
- [35] N. Bowden, S. Brittain, A. G. Evans, J. W. Hutchinson, G. M. Whitesides, *Nature* **1998**, *393*, 146.